Dynamic response of a wind turbine wake subjected to surge and heave step motions under different inflow conditions

Antonin Hubert, Boris Conan, Sandrine Aubrun

▶ **To cite this version:**

Antonin Hubert, Boris Conan, Sandrine Aubrun. Dynamic response of a wind turbine wake subjected to surge and heave step motions under different inflow conditions. The Science of Making Torque from Wind (TORQUE 2024), University of Firenze; European Academy of Wind Energy, May 2024, Florence, Italy. pp.092035, 10.1088/1742-6596/2767/9/092035 . hal-04621221

HAL Id: hal-04621221
https://hal.science/hal-04621221

Submitted on 23 Jun 2024

HAL is a multi-disciplinary open access archive for the deposit and dissemination of scientific research documents, whether they are published or not. The documents may come from teaching and research institutions in France or abroad, or from public or private research centers.

L'archive ouverte pluridisciplinaire **HAL**, est destinée au dépôt et à la diffusion de documents scientifiques de niveau recherche, publiés ou non, émanant des établissements d'enseignement et de recherche français ou étrangers, des laboratoires publics ou privés.

Distributed under a Creative Commons Attribution 4.0 International License

Journal of Physics: Conference Series

PAPER • OPEN ACCESS

Dynamic response of a wind turbine wake subjected to surge and heave step motions under different inflow conditions

To cite this article: Antonin Hubert *et al* 2024 *J. Phys.: Conf. Ser.* **2767** 092035

View the article online for updates and enhancements.

You may also like

- CFD analysis of the performance of different airfoils in ground effect
Zubin Zaheer, K E Reby Roy, Gopakumar S Nair et al.
- Investigation of modified AD/RANS models for wind turbine wake predictions in large wind farm
L L Tian, W J Zhu, W Z Shen et al.
- Swimming near the substrate: a simple robotic model of stingray locomotion
Erin Blevins and George V Lauder

This content was downloaded from IP address 90.107.123.132 on 23/06/2024 at 17:46

Journal of Physics: Conference Series **2767** (2024) 092035 doi:10.1088/1742-6596/2767/9/092035

Dynamic response of a wind turbine wake subjected to surge and heave step motions under different inflow conditions

Antonin Hubert[1], **Boris Conan**[1] **and Sandrine Aubrun**[1]

[1] Nantes Université, École Centrale Nantes, CNRS, LHEEA, UMR 6598, F-44000 Nantes, France

E-mail: antonin.hubert@ec-nantes.fr

Abstract.

The development of floating offshore wind turbines poses new challenges since the floating platform introduces complex dynamics in the wind turbine wake. These wake dynamics are intricately tied to the advection velocity, referring to the velocity of the downstream propagation of the air flow, and used in the context of wind farm modelling. The present article investigates the far-wake dynamic response of a wind turbine model subjected to heave (up-down translation) and surge (fore-aft translation) step motions under two distinct inflow conditions. Wind tunnel experiments were conducted with hot-wires in a realistic turbulent inflow and a low shear and no ground effect inflow, achieved by varying the hub height of the wind turbine model in the atmospheric boundary layer developed in the test section. The results show that the dynamic response of the wake under the low shear and no ground effect inflow conditions aligns with a second-order system with the presence of undershoots and overshoots. In contrast, under realistic conditions, it appears like a first-order system with undershoots and overshoots less evident in most cases. Despite these variations the determined advection velocity remains roughly the same and consistent with the literature for both heave and surge step motions, regardless of the inflow conditions.

1. Introduction

As the global demand for energy continues to rise, the development of new electricity production technologies becomes essential. Floating offshore wind turbines (FOWTs) have emerged as a promising solution due to their strategic locations, offering higher and more constant wind velocities and resulting to an increased capacity factor. While the wakes of bottom-fixed wind turbines have already been extensively studied [1–3], the dynamics involved in the context of a floating platform introduce new challenges and several questions persist, due to the youth of FOWT technologies.

A basic assumption for dynamic wake modelling is that flow structures contained in the wake are passively transported in the atmospheric flow, governed by an advection velocity U_a, in accordance with Taylors's frozen turbulence hypothesis [4]. This measure holds significant importance in unsteady wind farm modelling in general, as in FLORIDyn or FAST.Farm [5, 6]. FLORIDyn model assumed that observation points - *i.e.* the points where the wake dynamics are defined - propagate with an advection velocity equals to the freestream wind. FAST.Farm software assumes that the wake advects at the local spatially averaged the disturbed wind, but

Content from this work may be used under the terms of the Creative Commons Attribution 4.0 licence. Any further distribution of this work must maintain attribution to the author(s) and the title of the work, journal citation and DOI.
Published under licence by IOP Publishing Ltd

other models specified the advection velocity by various values. A straightforward approach is to set it equal to the mean free-stream velocity at hub height U_{hub} [7,8]. However, considering the reduced wind speed within the wake, the advection velocity is likely lower than the incoming free wind speed. Therefore, alternatives include setting it at a lower value, such as $0.8U_{\text{hub}}$ [9,10], or at an average value between the mean free-stream velocity and the mean wake velocity [8,11–13].

Previous studies have conducted experiments to determine the advection velocity value. In [9], the authors estimated it thanks to the meandering phenomenon, using a Doppler lidar. The advection velocity exhibited different values in two regions: $0.49U_{\text{hub}}$ between $2D$ to $3D$ and $0.55U_{\text{hub}}$ between $3D$ to $4D$, with D the diameter of the turbine. Another study using Doppler lidar experiments showed different results, with advection velocities between $0.7U_{\text{hub}}$ and $0.9U_{\text{hub}}$ [14]. Hot-wire experimentations with a turbine model subjected to yaw manoeuvres were performed in [15]. The results showed that, for a positive yaw manoeuvre - *i.e.* misaligning wind turbine with wind - the advection velocity is close to the free-stream velocity U_{hub}, while for negative one it is approximately $0.8U_{\text{hub}}$.

Several numerical and experimental studies have been performed and showed the impact of the floating motion on the wake of a FOWT [16–18]. The development of FOWT farms requires new wind wake models, and emphasizing the crucial need to understand the advection of these new dynamics. The present study aims to analyse the dynamic response of a wind turbine model subjected to heave (up-down translation) and surge (fore-aft translation) step motions, two predominant movements of a floater subjected to parallel wind-waves, to analyse the impact of the inflow in these dynamics and to retrieve the associated advection velocity. In this work, hot-wires (HW) experiments are conducted downwind of a porous disc under an atmospheric boundary layer (ABL) with realistic turbulent inflow. Two configurations are defined using the hub height of the turbine model, one with realistic turbulence and shear and one distant from the ground in order to reduce the shear and the ground effect. Since the hot-wires do not permit the interpretation of the steady state, caused by the absence of sufficient spatial distribution, the analysis is only performed on the transient phenomena.

The methodology is explained in section 2 where both configurations, the experimental set-up and the post-processing are detailed. Section 3 introduces the main results of the study, section 4 presents the result analysis and section 5 gives a brief conclusion to this work.

2. Methodology

2.1. Atmospheric boundary layer physical modelling

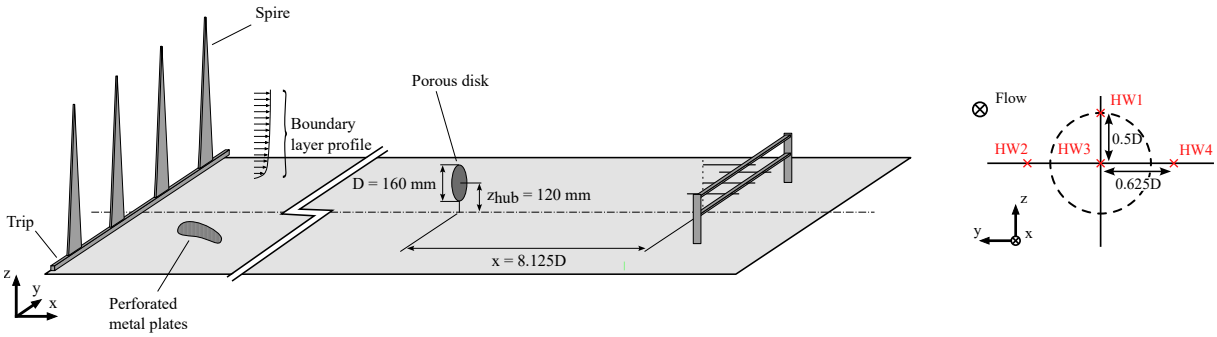

Figure 1. Experimental set-up in the atmospheric boundary layer wind tunnel (left panel), and hot-wires installation in the wind tunnel compared to the porous disc position (right panel).

Experiments are conducted in the ABL wind tunnel of the LHEEA laboratory (*research laboratory in hydrodynamics, energetics and atmospheric environment*) at École Centrale Nantes, in France. It is a 2 m × 2 m × 24 m test section facility, as presented on Figure 1. A 1:500 neutral

marine ABL is developed thanks to a trip and spires installed at the wind tunnel entrance and perforated metal plates placed all along the test section.

The resulting velocity profile, after a development fetch of 18 m, corresponds to an ABL above a slightly rough terrain according to [19] with, at full scale, a roughness length $z_0 = 5.7 \times 10^{-3}$ m, a power-law exponent $\alpha = 0.11$ and a zero-plane displacement $d_0 = 0$ m. Regarding the turbulence, the integral length-scale is about ${}^xL_u = 240$ m at hub height, while the target one is ${}^xL_u = 250$ m.

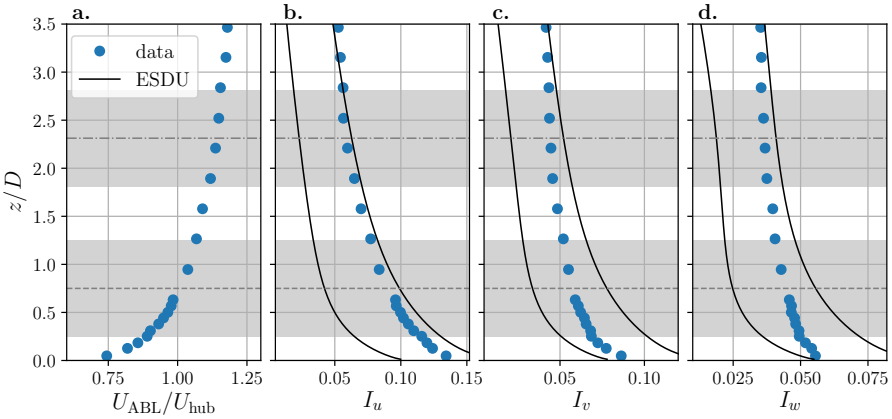

Figure 2. normalised mean velocity **(a)** and turbulence intensity profiles in the wind tunnel in the horizontal **(b)**, transversal **(c)** and vertical **(d)** direction. The grey areas represent the turbine model height ranges (with gray dashed and dotted-dashed lines representing the hub height for both configurations) and the black lines are the limits of ESDU [19] for a slightly rough terrain (from [20]).

Figure 2 show the resulting freestream velocity profile U_{ABL} normalised by the velocity at hub height $U_{\mathrm{hub}} = 3.0$ m/s for $z_{\mathrm{hub}} = 120$ mm, and the turbulence intensity profiles defined as: $I_i = \sigma_i / U_{\mathrm{ABL}}$ where $i = u\ v$ or w. More details on the turbulence and globally on the wind tunnel set-up are in [20].

2.2. Experimental set-up and data processing

The wind turbine model is a 1:500 reduced-scale of the 2 MW floating wind turbine FLOATGEN - 80 m of diameter, 60 m of hub height. It is a porous disc with a solidity of $\sigma = 57\%$ and a thrust coefficient of $C_t = 0.65$ [21]. It has a diameter of $D = 160$ mm, corresponding to a blockage ratio of 0.5%, and a hub height of $z_{\mathrm{hub}} = 120$ mm or $z_{\mathrm{hub}} = 370$ mm, depending of the configuration. The hub height of $z_{\mathrm{hub}} = 120$ mm corresponds to the 1:500 reduced-scale of FLOATGEN. For the following parts, config 1 is the configuration with the porous disc hub height set to $z_{\mathrm{hub}} = 120$ mm and config 2 the one with $z_{\mathrm{hub}} = 370$ mm. Table 1 summarizes the parameters values of the two experimental configurations used in this study. $\Delta U_{\mathrm{ABL}}/U_{\mathrm{hub}}$ represents the ABL velocity difference at the limits of the porous disc normalised by the hub height velocity for both configurations.

A 3-Degrees-of-Freedom (DoF) system placed under the wind tunnel test section is used to impose and acquire, with an acquisition frequency of 15 kHz, the step motions applied to the porous disc. For both configurations, in addition to a fixed case used as reference, surge (x translation) and heave (z translation) step motions are studied, with an amplitude modification of $\Delta x = \Delta z = 0.25D$ and a movement duration of $\Delta\tau^*_{\mathrm{m}} = 1.7$, with $\Delta\tau^*_m = \frac{\Delta\tau_{\mathrm{m}}}{\tau_0}$ the ratio between the manoeuvre time and the characteristic aerodynamic timescale based on the disc diameter and the velocity at hub height $\tau_0 = \frac{D}{U_{\mathrm{hub}}}$.

Table 1. Experimental configurations.

Parameters	config 1	config 2
z_{hub}	120 mm	370 mm
U_{hub}	3.0 m/s	3.4 m/s
$\Delta U_{\text{ABL}}/U_{\text{hub}}$	0.42	0.11
$[I_u, Iv, Iw]$	[0.09,0.06,0.05]	[0.06,0.05,0.04]
${}^{x}L_u$	240 m	260 m

Four Dantec 55-P11 probes (HW1-4), calibrated every day, and a pitot tube are installed $8.125D$ downstream of the porous disc, as shown in Figure 1 (right). The pitot tube is located at hub height, $3D$ from the hub center at the HW2 side, and measures the inflow hub height velocity. The calibration curve is fitted using the coefficients of King's Law [22], and pressure and temperature corrections are applied to the data. For all hot-wires, the χ^2 goodness of fit value is about 1×10^{-5} and 1×10^{-3} for config 1 and 2, respectively. The acquisition frequency is set to 15 kHz during an acquisition time of 2400 s and 1800 s for config 1 and 2, respectively. A digital low-pass Butterworth filter with a cut-off frequency set to 1 kHz is used in order to limit noise.

As the inflow has a high level of turbulence, a single step motion is inefficient to provide significant results. Consequently, a phase-averaging method synchronized with the porous disc step motions is performed on the data. Each motion case is divided into two step motions - ascent/descent for heave and backward/forward for surge - which are performed alternatively in time, but studied separately after phase-averaging. The acquisition times permit 600 and 450 motion steps in phase-averaging calculation for config 1 and config 2, respectively. The resulting phase-averaged velocities and x and z disc positions are noted $\widetilde{u}, \widetilde{x}, \widetilde{z}$.

2.3. Metrics for wake dynamics

To characterize the step motion effects, this study employs various normalised times and velocities. Establishing a standardized protocol is essential to accurately capture the transient duration, start and end times of these impacts.

U_{start} and U_{end} are the time-averaged velocities when the turbine model is at its first and second positions, respectively. The first position is defined as the original position of the porous disc before the motion and the second is its position after the motion. These velocities are calculated with the last third of phases present in the phase-averaged signal before the next motion.

The transient start τ_{start} is defined as the first time when the curve crosses a threshold value Δu_{th} compared to the averaged velocity before the step motion, and the transient end τ_{end} as the last time the curve crosses the same threshold value compared to the averaged velocity after the step motion U_{start}. The threshold value is set to $\Delta u_{\text{th}} = 0.07 U_{\text{hub}}$, as the smallest value ensuring the impact detection without any ambiguity. Dimensionless values are obtained by dividing both times by the aerodynamic timescale $\tau_0 = \frac{D}{U_{\text{hub}}}$: $\tau^*_{\text{start}} = \frac{\tau_{\text{start}}}{\tau_0}$ and $\tau^*_{\text{end}} = \frac{\tau_{\text{end}}}{\tau_0}$.

The dimensionless transient duration $\Delta\tau^*_{\text{i}}$ represents the total duration of the step impact. It is defined as the time difference between τ^*_{start} and τ^*_{end}: $\Delta\tau^*_{\text{i}} = \tau^*_{\text{end}} - \tau^*_{\text{start}}$. The ratio of this value and the motion duration is also used in this study: $\Delta\tau^*_{\text{ratio}} = \frac{\Delta\tau^*_{\text{i}}}{\Delta\tau^*_{\text{m}}}$.

The last metric used is the advection velocity. It represents the velocity at which the step effects are transported within the flow and is calculated with the delay between the start of the

step motion and its first impact in the wake at $\Delta x = 8.125D$ downstream of the turbine model: $U_{\mathrm{a}} = \frac{\Delta x}{\tau_{\mathrm{start}}}$.

3. Results

3.1. Experimentations for configuration 1, with shear and ground effect

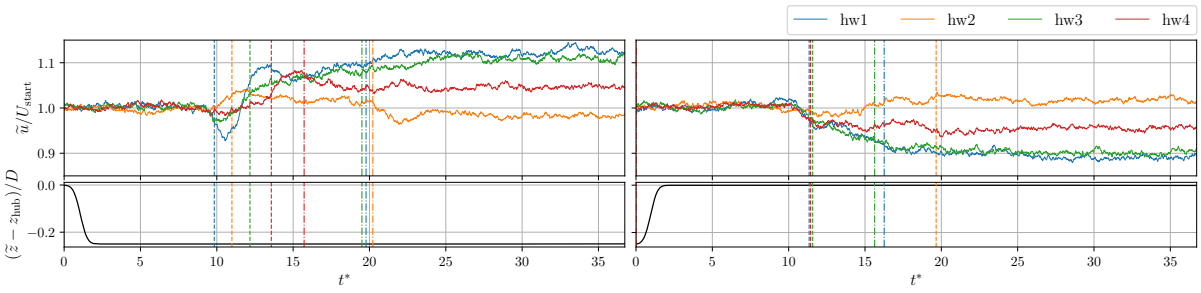

Figure 3. Phase-averaged velocities in the wake of a porous disc located at $z_{\mathrm{hub}} = 120$ mm and subjected to heave descent (left) and ascent (right) step motions. The dashed and dash-dotted vertical lines are the start times (τ^*_{start}) and end times (τ^*_{end}) of the step impact, respectively.

Figure 3 shows the four phase-averaged velocities normalised by U_{hub} for the turbine model subjected to heave step motions in config 1, with $t^* = \frac{t}{\tau_0}$ the normalised time. The dashed and dash-dotted lines represent the start times τ^*_{start} and end times τ^*_{end} of the step impact assessed as explained in Section 2.3, respectively.

During the transient phase of the ascent step (Figure 3 right), the velocities goes gradually back to the mean velocity U_{end}. The velocities present neither overshoots nor undershoots, similar to a first-order dynamic system. While for the descent step, the velocities exhibit various patterns depending of the probe's position. HW1 and HW3 velocity undershoot before reaching its U_{end} velocity, and HW2 and HW4 overshoot, attributed rather to a second-order dynamic system.

Theoretically, HW2 and HW4, located in symmetric transversal locations, should present the same steady state values. One can notice that it is not presently the case. As in previous studies [23, 24], a small negative transversal velocity exists in the wind tunnel, shifting the wake to the left, and resulting, $8.125D$ downstream, in a visible misalignment of the wake relative to hot-wires locations. Yet, consequences are limited for the analysis of the transient phenomena.

During the heave motion, when the porous disc descents, HW1 exits the wake and HW3 departs from the wake center, where the velocity deficit is maximum. On the other hand, HW2 and HW4 are initially positioned at the lateral wake boundaries during the first position, which barely change in the second step. This explains the challenges associated with determining the start and end times for these two hot-wires. The minimal differences pose difficulties in accurately capturing the actual impact times of the step motion. Obtaining the times for HW2 is difficult during the descent of the porous disc, whereas for HW4 this issue appears during its ascent. Thus, the analysis will be performed essentially on HW1 and HW3 time series for all heave motion cases, which are more evident.

Figure 4 shows the four phase-averaged velocities normalised by U_{hub} for the turbine model subjected to surge step motion in config 1. As for Figure 3, the dashed and dash-dotted lines represent the start times τ^*_{start} and end times τ^*_{end} of the step impact assessed as explained in Section 2.3, respectively.

The influence of the surge backward step appears to be less significant compared to the forward step, particularly for HW3 with its more important start time $\tau^*_{\mathrm{start}} = 17.1$. And, as

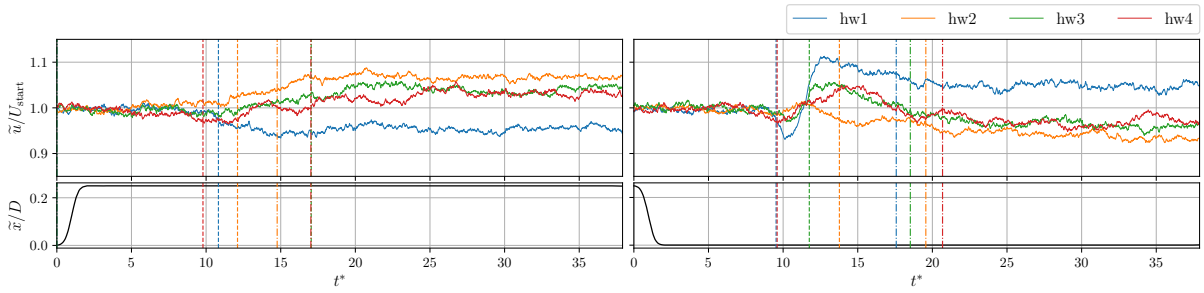

Figure 4. Same as Figure 3 but for surge backward (left) and forward (right) step motions.

in heave step motions, surge step motions exhibit difficulties in accurately capturing the actual impact times. Only HW4 seems to provide precise results during forward phase, so the analysis for surge step motions will be performed essentially on HW1 and HW4 times for all surge motion cases.

Table 2. Dynamic wake metrics in config 1 - Signal of HW1,HW3 are used for heave step motions and HW1,HW4 for surge ones

Step motion	τ^*_{start}	τ^*_{end}	$\Delta\tau^*_{\text{i}}$	$\Delta\tau^*_{\text{ratio}}$	$U_{\text{a}}/U_{\text{hub}}$
heave descent	9.92, 12.12	19.83, 19.46	9.92, 7.35	6.75, 5.00	0.82, 0.67
heave ascent	11.38, 11.57	16.34, 15.61	4.96, 4.04	3.38, 2.75	0.71, 0.70
surge backward	10.80, 9.85	— , 17.06	— , 7.20	— , 4.75	0.75, 0.82
surge forward	9.48, 9.66	17.62, 20.66	8.15, 10.99	5.38, 7.25	0.86, 0.84

Table 2 shows the transient times of the dynamic response of the wake to heave and surge step motions in config 1. The absence of τ^*_{end} for HW1 is related to the capture protocol described in Section 2.3. Specifically, in this case τ^*_{end} is determined after τ^*_{start} and is, therefore, not applicable. Moreover, the other transient times $\Delta\tau^*_{\text{i}}$ and $\Delta\tau^*_{\text{ratio}}$, calculated with τ^*_{end}, are also not applicable in this case.

The start times are different between the descent and ascent heave steps. Based on HW1 values, the first one exhibits $\tau^*_{\text{start}} \approx 10$, while the second one $\tau^*_{\text{start}} \approx 11.5$. The $\tau^*_{\text{start}} = 12.12$ value for HW3 in case of heave descent step is attributed to an incorrect impact detection, as modifications are visible as early as $t^* \approx 10$ in Figure 3. These start times result in advection velocities of $U_{\text{a}} = 0.81U_{\text{hub}}$ for the descent step and $U_a = 0.71U_{\text{hub}}$ for the ascent one. These values are close to those reported in [15] for a negative yaw manoeuvre.

The start times found in surge step motions are close to those in heave descent ones, either in backward or in forward steps: both cases show $\tau^*_{\text{start}} \approx 10$. Indeed, surge motions do not involved aerodynamics timescale change, unlike heave ones. This start time value gives an advection velocity of $U_{\text{a}} \approx 0.81$ for both backward and forward steps, aligning with the one found in heave descent step.

The end times are $\tau^*_{\text{end}} \approx 19.5$ for descent step, displaying a longer impact compared to ascent step, which exhibit $\tau^*_{\text{end}} \approx 16$. For the descent step, only the HW4 deviates from the other results. As seen before, it is also the only one with a distinct start time. This suggests the possibility that HW4 is less affected by the step compared to the other hot-wires. These values give transient durations of $\Delta\tau^*_{\text{i}} \approx 8$ and $\Delta\tau^*_{\text{i}} \approx 4.5$, and a ratio of $\Delta\tau^*_{\text{ratio}} \approx 5.5$ and $\Delta\tau^*_{\text{ratio}} \approx 3$ for descent and ascent step, respectively.

The end times of surge step motions are more grouped compared to heave ones, included in $\tau^*_{\text{end}} \in [17 : 20.7]$, and resulting in $\Delta\tau^*_{\text{i}} \in [7.2 : 11]$ and $\Delta\tau^*_{\text{ratio}} \in [4.8 : 7.3]$.

3.2. Experimentations for configuration 2, neither shear nor ground effect

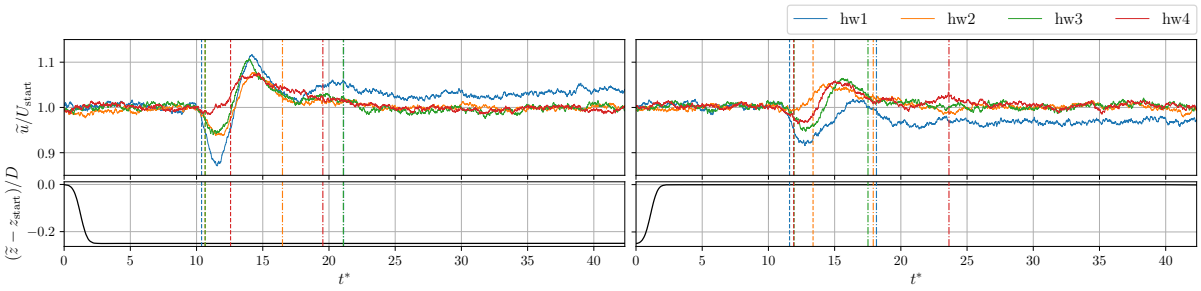

Figure 5. Phase-averaged velocities in the wake of a porous disc located at $z_{\text{hub}} = 370$ mm and subjected to heave descent (left) and ascent (right) step motions. The dashed and dash-dotted vertical lines are the start times (τ^*_{start}) and end times (τ^*_{end}) of the step impact, respectively.

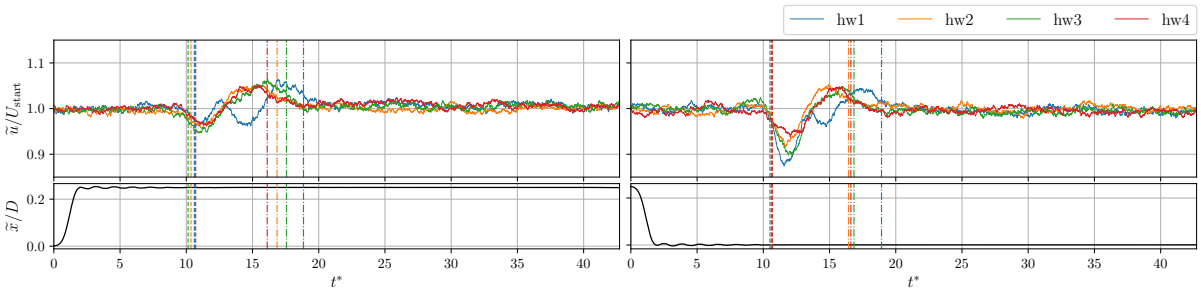

Figure 6. Same as Figure 5 but for surge backward (left) and forward (right) step motions.

Figures 5 and 6 show the four phase-averaged velocities normalised by U_{hub} for the turbine model subjected to heave and surge step motions in config 2, respectively. As for the figures in Section 3.1, the dashed and dash-dotted lines represent the start times τ^*_{start} and end times τ^*_{end} of the step impact founded as explained in Section 2.3, respectively. In the scenario of surge step motion, the position of the porous disc is slightly unstable after the step, leading to persisting oscillations until $t^* = 10$. This instability is attributed to the longer mast, the 3DoF system has difficulties to establish a stable position due to this additional weight and the higher lever arm. However, these instabilities remain minimal $8.125D$ downstream of the turbine model as the maximum amplitude of these oscillations is about $0.03D$. No consequences are expected.

In comparison to the findings in config 1, the dynamics are more pronounced in config 2. The undershoots and overshoots are present for all hot-wires and in both surge and heave step motions, similar to a second-order dynamic system. The maxima and minima reaching a velocity gap with the mean velocity of $0.13U_{\text{hub}}$, while in config 1 these values are approximately $0.06U_{\text{hub}}$. This greater dynamic responses in config 2 are attributed to the lower turbulence levels in the inflow, resulting in reduced mixing effects. In the surge step motion scenarios, HW1 displays several consecutive undershoots and overshoots.

Table 3 shows the transient times of the dynamic response of the wake to descent and ascent heave step motions in config 2.

Table 3. Dynamic wake metrics in config 2 - HW1,HW3 for heave step motions and HW1,HW4 for surge ones

Step motion	τ^*_{start}	τ^*_{end}	$\Delta\tau^*_{\text{i}}$	$\Delta\tau^*_{\text{ratio}}$	$U_{\text{a}}/U_{\text{hub}}$
heave descent	10.37, 10.68	21.17, 21.17	10.80, 10.58	6.38, 6.25	0.78, 0.76
heave ascent	11.64, 11.85	18.21, 17.57	6.56, 5.72	3.88, 3.88	0.70, 0.69
surge backward	10.68, 10.68	18.79, 16.02	8.12, 5.34	4.75, 3.13	0.76, 0.76
surge forward	10.46, 10.68	19.01, 16.66	8.54, 5.98	5.00, 3.50	0.78, 0.76

In the case of config 2, the start times barely change across all scenarios, with a value of $\tau^*_{\text{start}} \approx 10.5$, except for ascent step which has $\tau^*_{\text{start}} \approx 11.8$ as observed earlier. In case of heave step motions, some hot-wires display higher start times (HW4 for descent step and HW2 for ascent) potentially caused by the absence of undershoot.

The corresponding advection velocities for these values are $U_{\text{a}} \approx 0.77U_{\text{hub}}$ and $U_{\text{a}} = 0.69U_{\text{hub}}$, respectively. These results align those identified in config 1, despite the different inflow conditions. In [15], the authors founded similar values in case of yaw manoeuvres. This result highlights the universality of the advection velocity values in the context of step motions.

Globally, the results show end times between $\tau^*_{\text{end}} \in [16 : 21]$, as for config 1. The scatter is higher for end times compared to start times, depending of the hot-wire, but descent step shows higher end times with $\tau^*_{\text{end}} \approx 21$. Those end times result in $\Delta\tau^*_{\text{i}} \in [5.3 : 10.6]$ and $\Delta\tau^*_{\text{ratio}} \in [3.1 : 6.4]$, in the order of magnitude of those in config 1.

4. Discussion

The start times are different between the descent and ascent steps for both configurations, $\tau^*_{\text{start}} \approx 10$ and $\tau^*_{\text{start}} \approx 11.5$ respectively, which is surprising since the two heave step motions are symmetric. This could be attributed to the changing velocity at hub height when the porous disc is at its permanent positions, consequently affecting the aerodynamics timescale τ_0. The layers closest to the ground possess a lower aerodynamic timescale, involving a lower advection velocity. Moreover, the velocity difference between the height extrema is more pronounced when the porous disc is at its lowest position compared to its highest, caused by the higher shear level. Consequently, the advection velocity of the ascent step, as for the descent step but to a lesser degree, may be underestimated.

Considering Figure 2, the inflow velocity at hub height when the porous disc is at its lowest position is $U = 0.89U_{\text{hub}}$, resulting in a corrected $\tau_{0\_\text{corrected}} = 0.06$ s, instead of $\tau_0 = 0.05$ s. The start time of HW1 would result in $\tau^*_{\text{start\_corrected}} = 10.2$ for the ascent step, slightly higher than the $\tau^*_{\text{start}} = 9.9$ for the descent step which seems reasonable. However, while this explanation is suitable for config 1, it is not for the differences observed in config 2, where shear is almost negligible. In config 2, the start time of HW1 would result in $\tau^*_{\text{start\_corrected}} = 11.2$ (instead of 11.6) for the ascent step, significantly deviating from the descent step value of $\tau^*_{\text{start}} = 10.1$. Consequently, this observed difference can only be attributed to the nature of the step motion itself. However, this thought experiment highlights the sensitivity of the start time to the inflow conditions.

Distinct velocity dynamics are evident in backward and forward steps in config 1 (Figure 4). Specifically, the backward step exhibits neither undershoot nor overshoot, in contrast to the forward step, where it is especially noticeable for HW1. These observations are close to heave step motion case findings, where the ascent step also shows neither undershoot, nor overshoot. However these differences may be caused by the dynamics involved in the wake. In contrast, for

config 2 all hot-wires in all motion cases present overshoots and undershoots. The absence of shear and of ground effect remain the dynamics visible up to $8.125D$ downstream of the turbine model.

In [25], the authors performed numerical and experimental investigations of the flow over a disc subjected to surge motion (with $\Delta\tau^*_{\mathrm{m}} = 4.3$). They observed that disc movement generates a growing ring vortex at the edges of the disc. In [26], they looked at the wake development of a porous disc under transient load (with $\Delta\tau^*_{\mathrm{m}} = 0.2, 0.4, 0.8$), which can be assimilated to surge step, and found the formation of a ring vortex growing as it goes downstream. The undershoots and overshoots present in surge step motions may be the passage of this ring vortex.

The observed undershoots and overshoots in heave step motions, visible in Figure 3 and particularly evident in Figure 5, can be associated to a deflection of the wake. The heave step motions of the porous disc induces a relative angle between the inflow and the porous disc of approximatively 10° and 8.5° for config 1 and 2, respectively.

Numerical and experimental previous studies have reported that, at $x = 8D$, wake deflections reach $y = 0.2D$ to $0.35D$ for yaw angle of 10°, depending of the study [27–29]. The brief motion time during which the porous disc exhibits a relative angle with the inflow can be similar to a pitch angle case, and results in these observed undershoots and overshoots.

5. Conclusion

This study aims to answer the question of advection velocity in the context of dynamic wake model development by conducting wake dynamics measurements. Hot-wire experiments were performed $8.125D$ downstream of a porous disc subjected to heave and surge step motions, under a neutral marine atmospheric boundary layer. Two configurations of hub height were tested - with shear and ground effect ($z_{\mathrm{hub}} = 120$ mm) and without ($z_{\mathrm{hub}} = 370$ mm) - to explore the influence of the inflow velocity and turbulence on wake transient times. Several observations were drawn:

- Undershoots and overshoots, representative of a second-order dynamic system, are visible for all hot-wires in all cases in the configuration with low shear and low ground effect (config 2). In contrary, in the configuration with higher turbulence level and shear (config 1), these are no longer evident for all hot-wires and the impact of the step motion aligns with a damped system.
- The inflow conditions barely change the transient times, nor the advection velocity values: for ascent step $U_{\mathrm{a}} \approx 0.7U_{\mathrm{hub}}$ and for the descent step and surge step motions, $U_{\mathrm{a}} \approx 0.8U_{\mathrm{hub}}$. This difference could be attributed to the motion itself, and not to the velocity shear as it remains visible regardless of its presence.
- The influence of step motions persists for a duration longer than the motion itself, regardless of the motion and the inflow conditions. The average ratio $\Delta\tau^*_{\mathrm{ratio}}$ are essentially between 3 and 6, indicating that the impact duration is 3 to 6 times longer than the duration of the manoeuvre, and can extend to 7 times for some cases.

Future investigations are essential as the porous disc does not faithfully represent a wind turbine. The presence of tip vortices could potentially alter the observations and the values of advection velocity determined here in the far-wake. Moreover, to enhance the comprehension of the involved phenomena, conducting experiments with higher spatial resolution, such as time-resolved PIV, could be valuable given the rapid nature of the step motions.

References

[1] Vermeer L J, Sørensen J N and Crespo A 2003 *Progress in Aerospace Sciences* **39** 467–510 ISSN 0376-0421
[2] Larsen G C *et al.* 2007 Dynamic wake meandering modeling Tech. Rep. Risø-R-1607(EN) Risø National Laboratory

[3] Porté-Agel F, Bastankhah M and Shamsoddin S 2020 *Boundary-Layer Meteorol.* **174** 1–59 ISSN 0006-8314, 1573-1472
[4] Taylor G I 1938 *Proc. R. Soc. Lond. A* 476–490 ISSN 0080-4630
[5] Jonkman J and Shaler K 2021 FAST.Farm User's Guide and Theory Manual Tech. Rep. NREL/TP-5000-78785 Golden, CO: National Renewable Energy Laboratory
[6] Becker M *et al.* 2022 *Wind Energy Sci.* **7** 2163–2179 ISSN 2366-7451
[7] Trujillo J J, Bingöl F, Larsen G C, Mann J and Kühn M 2011 *Wind Energy* **14** 61–75 ISSN 1099-1824
[8] Shapiro C R, Starke G M, Meneveau C and Gayme D F 2019 *Energies* **12** 2956 ISSN 1996-1073
[9] Machefaux E *et al.* 2015 *Wind Energy* **18** 2085–2103 ISSN 10954244
[10] De Maré M 2015 *Wake Dynamics in Offshore Wind Farms* 1st ed (Kgs. Lyngby: DTU Vindenergi) ISBN 978-87-93278-33-2
[11] Cheng W C and Porté-Agel F 2018 *Boundary-Layer Meteorol.* **169** 1–10 ISSN 0006-8314, 1573-1472
[12] Zong H and Porté-Agel F 2020 *J. Fluid Mech.* **889** A8 ISSN 0022-1120, 1469-7645
[13] Vahidi D and Porté-Agel F 2022 *Energies* **15** 9477 ISSN 1996-1073
[14] Brugger P, Markfort C and Porté-Agel F 2022 *Wind Energ. Sci.* **7** 185–199 ISSN 2366-7451
[15] Macrí S, Aubrun S, Leroy A and Girard N 2021 *Wind Energ. Sci.* **6** 585–599 ISSN 2366-7451
[16] Duan L, Sun Q, He Z and Li G 2022 *Energy* **260** 124907 ISSN 03605442
[17] Kleine V G *et al.* 2022 *Phys. of Fluids* **34** 074106 ISSN 1070-6631, 1089-7666
[18] Messmer T, Holling M and Peinke J 2023 *Wind Energ. Sci. Discussions (preprint)*
[19] ESDU 1985 Part II: Single point data for strong winds (neutral atmosphere) *Characteristics of Atmospheric Turbulence near the Ground* 85020 (London: ESDU International) ISBN 978-0-85679-526-8
[20] Schliffke B, Conan B and Aubrun S 2024 *Wind Energ. Sci.* **9** 519–532
[21] Aubrun S *et al.* 2019 *J. Phys.: Conf. Ser.* **1256** 012004 ISSN 1742-6588, 1742-6596
[22] King L V 1914 *Proc. R. Soc. Lond. A* **90** 563–570 ISSN 0950-1207, 2053-9150
[23] Raibaudo C *et al.* 2022 *J. Phys.: Conf. Ser.* **2265** 022085 ISSN 1742-6588, 1742-6596
[24] Schliffke B 2022 *Experimental Characterisation of the Far Wake of a Modelled Floating Wind Turbine as a Function of Incoming Swell* Ph.D. thesis Centrale Nantes Nantes
[25] Higuchi H, Balligand H and Strickland J 1996 *J. Fluids and Structures* **10** 705–719 ISSN 08899746
[26] Yu W, Ferreira C and van Kuik G 2019 *Renewable Energy* **132** 1402–1414 ISSN 09601481
[27] Jiménez Á, Crespo A and Migoya E 2010 *Wind Energy* **13** 559–572 ISSN 1095-4244, 1099-1824
[28] Bastankhah M and Porté-Agel F 2015 *J. Phys.: Conf. Ser.* **625** 012014 ISSN 1742-6588, 1742-6596
[29] Schottler J *et al.* 2017 *J. Phys.: Conf. Ser.* **854** 012032 ISSN 1742-6588, 1742-6596